

Observation of magnetic-field-sweep-direction-dependent dynamic nuclear polarization under periodic optical electron spin pumping

Michael Macmahon,¹ Joseph R. Iafate,² Michael J. Dominguez,² and Vanessa Sih^{1,*}

¹*Department of Physics, University of Michigan, Ann Arbor, Michigan 48109, USA*

²*Applied Physics Program, University of Michigan, Ann Arbor, Michigan 48109, USA*

Optical pump-probe techniques are used to generate and measure electron spin polarization in a gallium arsenide epilayer in which the electron spin coherence time exceeds the mode-locked laser repetition period. Resonant spin amplification occurs at magnetic fields at which the electron spin polarization excited by successive laser pulses add constructively. Measurements of Kerr rotation as a function of applied magnetic field reveal nuclear spin polarization that aligns either with or against the external magnetic field depending on whether the applied magnetic field is being decreased or increased. Furthermore, the nuclear spin polarization magnitude varies in proportion to the perpendicular net electron spin polarization as the latter changes due to resonant spin amplification and other causes. We also report an experimental technique that reveals a minutes-long memory of precise field history in the electron-nuclear spin system.

I. INTRODUCTION

The manipulation and hyperpolarization of nuclear spin holds particular interest for potential application in spin-based classical and quantum information processing [1–4]. Specifically, understanding how to control and optimize nuclear spin polarization could be applied to generate a hyperpolarization of nuclear spins to enhance magnetic resonance imaging and store information [1]. Furthermore, being able to control nuclear spin polarization would enable pathways for manipulating electron spin polarization and maximizing the electron spin coherence time for electron spin-based information processing [2–4].

The optical pumping of electron spins has been shown to generate dynamic nuclear polarization in bulk semiconductors [5, 6], quantum wells [7], and quantum dots [8]. Magneto-optical techniques can monitor this nuclear polarization through its effect (Overhauser field) on the electron spin system [6–8], including in the regime of resonant spin amplification (RSA) [9]. Recently, periodic Overhauser fields have been observed with Voigt geometry time-resolved Kerr rotation (TRKR) in fluorine-doped ZnSe [10, 11]. Although dynamic nuclear polarization is not expected in the Voigt geometry [12], the dynamic nuclear polarization in Ref. [11] is attributed to electron spins rotated into the magnetic field direction by the optical Stark effect. However, these experiments did not observe any dependence on the direction of the magnetic field sweep [11]. The optically-driven electron-nuclear spin system has also recently revealed interesting feedback effects in quantum dots; for example, the nuclear spin polarization has been found to adjust through a feedback mechanism in response to laser frequency [13] and applied microwave magnetic field [14].

In this paper, we report Kerr rotation for electron spins in gallium arsenide (GaAs) that unexpectedly depends on

the direction the magnetic field is swept. This is evidence of a nuclear spin polarization that depends on whether the applied magnetic field is increasing or decreasing. Furthermore, the magnitude of dynamic nuclear polarization changes in response to changes in the magnitude of the transverse electron spin polarization due to resonant spin amplification, both periodically with applied magnetic field and over time with the field held constant. Finally, we present an experimental technique of steeping during a sweep of external magnetic field and show that this produces a striking echo effect in the subsequent spin signal.

II. METHODS

The measurements were performed on a 2 μm thick Si-doped GaAs epilayer (doping density $n = 3 \times 10^{16} \text{ cm}^{-3}$) which was grown on top of a 1 μm thick undoped Al-GaAs epilayer, grown by molecular-beam epitaxy on an undoped (001) GaAs substrate. We mounted the sample in a helium flow cryostat to maintain the sample temperature at 10 K.

We optically generated and measured electron spin polarization via TRKR [15]. A mode-locked Ti:S laser with a repetition rate of 76 MHz, tuned near the band edge of GaAs, provided both the spin generation (pump) and measurement (probe) beams. A photoelastic modulator alternated the helicity of the pump beam between left- and right-circular polarization at 50 kHz. The linearly-polarized probe beam was chopped at 1.37 kHz and reflected off the sample before being split by a Wollaston prism and collected by two optical fibers (A and B) feeding into a photodiode bridge. The prism split the horizontal and vertical components of linear polarization, and a half-wave plate before the prism balanced the proportion of light entering fibers A and B in the absence of Kerr rotation. The photodiode bridge output of A – B corresponds to a direct measurement of Kerr rotation, and lock-in detection was used to filter signal modulated

* vsih@umich.edu

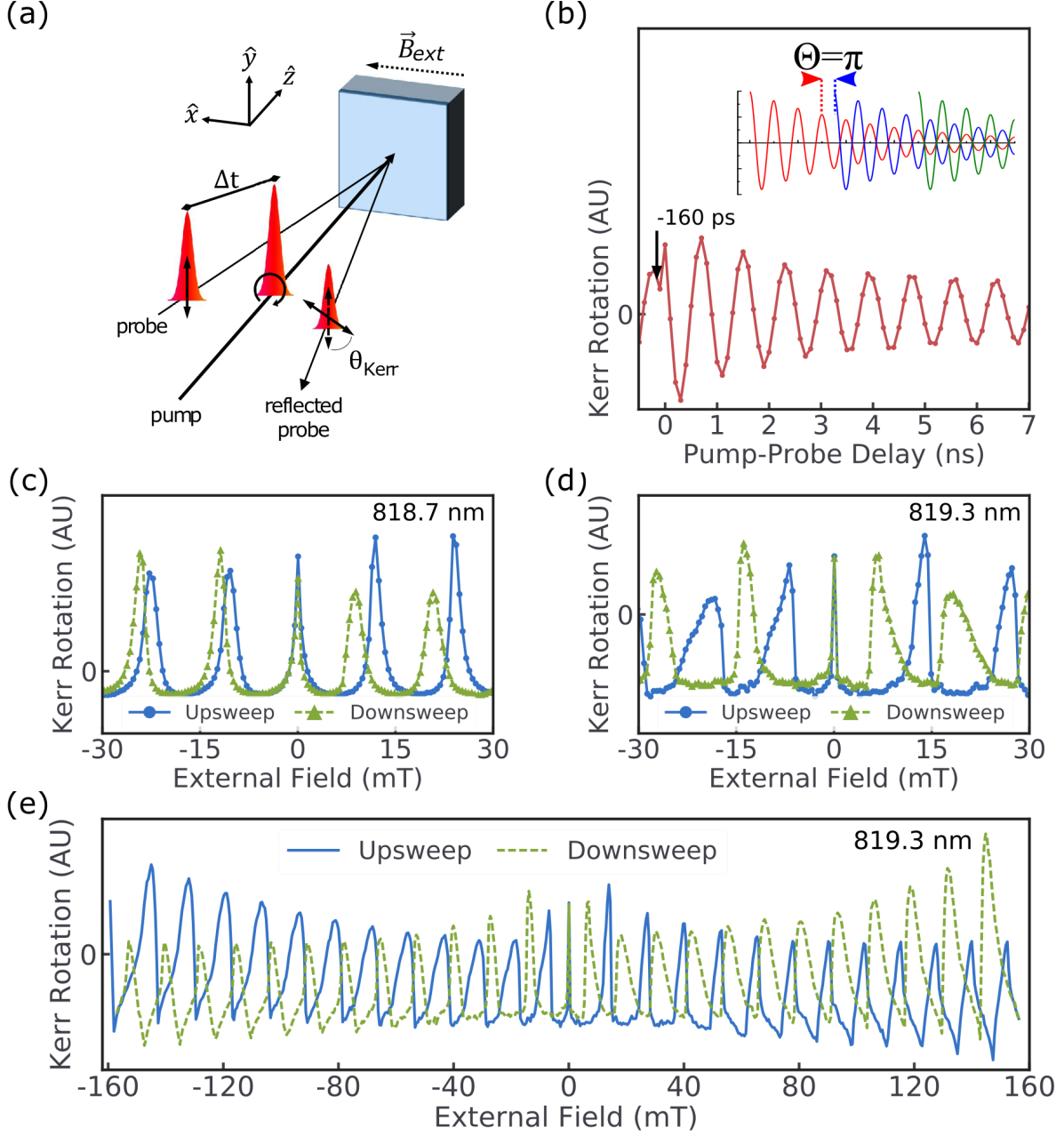


FIG. 1. (a) Experimental geometry for optical pump-probe Kerr rotation measurements. (b) Time-resolved Kerr rotation measured at laser wavelength 818.7 nm with external magnetic field $B_{ext} = 200$ mT. The arrow at -160 ps indicates the pump-probe delay used for magnetic field sweeps. Inset: Due to a spin coherence time longer than the laser repetition period, electron spin packets excited by consecutive laser pulses (denoted with different colors) interfere destructively when the product of Larmor precession frequency and pump-probe delay Θ equals π (modulo 2π). (c), (d) Kerr rotation measured as a function of external magnetic field, for a fixed pump-probe delay of 13 ns, at (c) 818.7 nm and (d) 819.3 nm. The field is swept from -160 mT to +160 mT for upsweeps and from +160 mT to -160 mT for downsweeps. For clarity, only data from -30 mT to +30 mT is shown. Excepting the peak at zero external field, upsweep peaks demonstrate a shift with respect to downsweep peaks. At certain laser wavelengths such as (d), the peaks take on a distinctly asymmetric profile absent in (c). (e) The full upsweep and downsweep excerpted in (d).

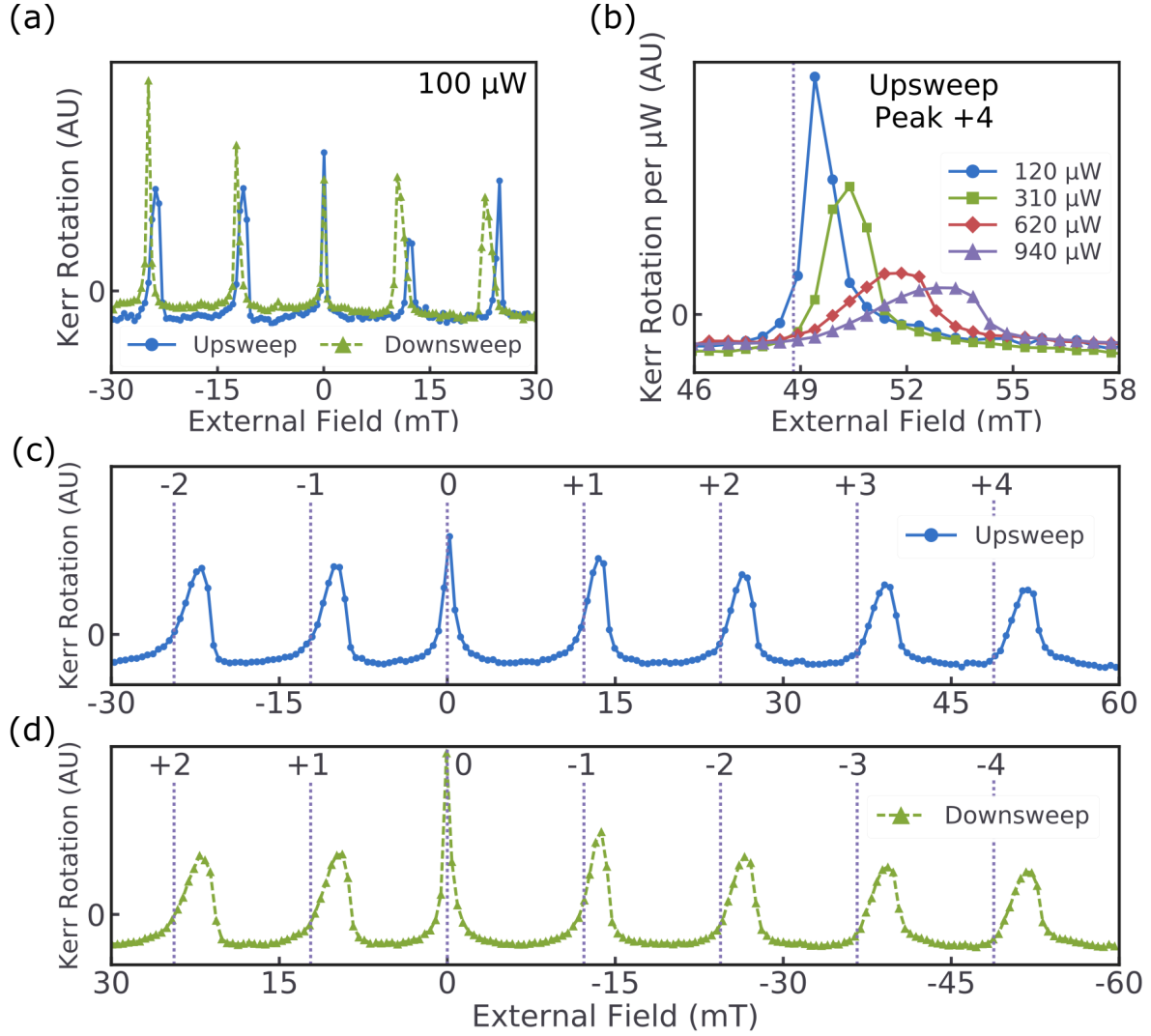


FIG. 2. (a) Kerr rotation as a function of B_{ext} , for a fixed pump-probe delay of 13 ns, performed with a lower pump power of 100 μW . The field is swept from -160 mT to +160 mT for upsweeps and from +160 mT to -160 mT for downsweeps. For clarity, only data from -30 mT to +30 mT is shown. The upsweep and downswipe peaks still shift with respect to one another but the peaks are no longer asymmetric in shape. (b) Peak +4 from (c) at four pump powers and incident probe power of 100 μW taken at 819.6 nm. The Kerr rotation values are normalized by pump power for comparison. As pump power increases, the peak deforms from the expected shape and shifts to a larger applied field. The dotted vertical line indicates the expected position of the RSA peak in the absence of DNP. (c), (d) Kerr rotation as a function of B_{ext} for a pump-probe delay of 13 ns. The peaks are labeled with respect to the peak at zero applied field. By plotting the two peaks encountered before zero and four peaks encountered after for both an (c) upsweep and (d) downswipe, we observe that the field sweep direction, and not sign, determines the shapes of the peaks. Note that the field axis in (d) is reversed. The dotted vertical lines indicate the expected positions of the RSA peaks in the absence of DNP.

at the frequencies of the photoelastic modulator and optical chopper.

Fig. 1(a) depicts the experimental geometry. Unless otherwise noted, measurements are performed with a laser wavelength of 819.3 nm and incident pump and probe powers of approximately 500 μW and 80 μW , respectively, measured before the cryostat. A mechanical delay line was used to vary the relative optical path length of the pump and probe beams for TRKR measurements. An electromagnet provided an external magnetic

field B_{ext} perpendicular to the optical axis. Electron spins precess about B_{ext} at the Larmor spin precession frequency $g\mu_B B_{ext}/\hbar$, resulting in the oscillations seen in Fig. 1(b).

To measure RSA in our sample, we set our delay line to achieve a 13 ns pump-probe temporal separation, equivalent to -160 ps in Fig. 1(b). We measured Kerr rotation every 1.1 s, incrementing the applied magnetic field by 0.5 mT for every other measurement. For clarity, field scans in Figs. 1-4 show only the second of each pair of

measurements at a given field. This allowed us to measure, as a function of these sweeps of the external field, the net spin polarization 13 ns after each pump pulse reaches the sample. To rule out hysteresis in our magnetic field as a cause of our results, we used a gaussmeter to measure the magnetic field at the sample location as the magnet underwent the same sequence and timing of field values as those used to collect the data, and the true, measured field is used in all figures.

III. RESULTS

As shown in Fig. 1(b), a significant Kerr rotation is present at negative pump-probe delay times, indicating a spin coherence time exceeding the 13.16 ns repetition period of the laser, T_{rep} . As a result, the electron spins generated by each laser pulse will constructively or destructively interfere with the remnants of those from previous pulses, depending on the product of Larmor frequency and T_{rep} . This phenomenon is referred to as resonant spin amplification (RSA) and can be used to monitor the electron spin dynamics [16, 17].

For most wavelengths and incident pump powers, the resulting pattern of Kerr rotation during a sweep of applied external magnetic field, measured at a fixed pump-probe time delay, consists of sharp peaks separated by $B_{ext} = h/(g\mu_B T_{rep})$ [16]. Peaks occur when the existing spin polarization is in phase with the polarization induced by the laser pulse each time it illuminates the sample, corresponding to $\Theta = 0$ in the inset of Fig. 1(b). The peak spacing and peak shape are generally identical

when sweeping up (negative to positive magnetic field) and down (positive to negative magnetic field). However, under certain measurement conditions, the phenomenon shown in Fig. 1(d,e) occurs in which all RSA peaks, except for the central peak at $B_{ext} = 0$, take on a distinctly asymmetric profile with a corresponding peak shift. Sweep direction, sweep speed, field history, and pump power all strongly affect the character of this peak warping.

Fig. 2 shows the effects of changing pump power and magnetic field polarity and sweep direction. As shown in Fig. 2(b), when the pump power increases, the peak location shifts to larger applied field, the peak width increases, and the peak shape becomes more asymmetric. From Fig. 2(c,d), we see that when the applied magnetic field is increasing in magnitude, the magnetic field experienced by the electrons is weaker than the one applied, causing each peak to shift to a stronger external field - and vice versa. Prior work has not reported differences in RSA between increasing and decreasing applied magnetic field [9–11, 16]. The equivalence of Fig. 2(c) and Fig. 2(d) confirms these differences depend only whether the external field increases or decreases, not upon which direction on-axis the field points.

In order to gain a qualitative understanding of this phenomenon, we will now present a phenomenological model. In RSA experiments with our experimental geometry and in the absence of DNP, the following equations adapted from Ref. [17] effectively model the time-averaged electron spin polarization component along the laser axis and thus the measured Kerr rotation:

$$\varphi_{Kerr}(B_{ext}, T_{delay}) \propto s_z(B_{ext}, T_{delay}) = s_r(B_{ext}) \cos(s_\varphi(B_{ext}, T_{delay})) \exp(-T_{delay}/T_e) \quad (1)$$

$$s_r(B_{ext}) = s_0(1 - 2 \cos(\Theta(B_{ext})) \exp(-T_{rep}/T_e) + \exp(-2 T_{rep}/T_e))^{-1/2} \quad (2)$$

$$s_\varphi(B_{ext}, T_{delay}) = (g\mu_B T_{delay}/\hbar)B_{ext} + \tan^{-1} \left(\frac{\exp(-T_{rep}/T_e) \sin(\Theta(B_{ext}))}{1 - \exp(-T_{rep}/T_e) \cos(\Theta(B_{ext}))} \right) \quad (3)$$

$$\Theta(B_{ext}) = (g\mu_B T_{rep}/\hbar)B_{ext} \quad (4)$$

where T_e is the electron spin lifetime, s_0 is the spin polarization magnitude, and s_z is the spin polarization along the optical axis \hat{z} . To reconcile Eq. (1) with the peak-warping we have discussed, we introduce an additional field B_N parallel to the external field B_{ext} that also acts on the electron spin system. Then, we substitute B_{ext} with $B_{ext} + B_N$ in Eqs. (1-4) and allow this new field to vary with a timescale T_N . Furthermore, we postulate that the magnitude of B_N never rises beyond a few mT. Under these conditions, B_N can be thought to lo-

cally shift, shrink, and stretch $\varphi_{Kerr}(B_{ext})$ and, when properly chosen, reproduce the qualitative features of the phenomenon shown in Figs. 1 and 2.

We choose the label B_N because we identify this field as the Overhauser field arising from dynamic nuclear polarization (DNP). In our phenomenological model, we propose that B_N obeys three heuristic properties that qualitatively reproduce the peak-warping seen in our experimental results. The properties are as follows:

1. B_N attempts to maintain a magnitude proportional to s_r as described in equation (2). This change is limited by the nuclear polarization timescale T_N .
2. B_N is zero in the vicinity of $B_{ext} = 0$ and the optical nuclear magnetic resonances of spin-polarized nuclear species.
3. B_N is aligned antiparallel to the external field when the external field magnitude increases, and parallel when the external field magnitude decreases.

The rest of the paper will discuss our model and the degree to which it is supported by our data. The magnitude of nuclear polarization dynamically rises and falls in response to changes in the magnitude of the electron spin polarization, but unlike the electron spins, the nuclear spins align collinear to the external magnetic field. This is Property 1. Note that the nuclear polarization we describe is specifically proportional to the component of electron spin polarization precessing in the plane perpendicular to B_{ext} , as it is only this component that undergoes RSA, and this paper demonstrates that the changes in electron spin polarization due to RSA determine the nuclear polarization.

Experimentally, Fig. 2(b) provides direct evidence that the magnitude of DNP is proportional to the magnitude of electron spin polarization. Each RSA peak occurs at a field satisfying $\Theta(B_{ext} + B_N) = 2n$ for integer n (see Eq. 4). As a result, the shift of each RSA peak in a sweep of B_{ext} gives a direct measurement of B_N , assuming the g-factor of the spins is constant (note that a change in g-factor would lead to a change in peak spacing that we do not observe). Because the magnitude of electron spin polarization is proportional to the power of the pump laser, we can interpret Fig. 2(b) as indicating a correlation between nuclear polarization and electron spin polarization, providing support to Property 1.

When the external magnetic field approaches zero, nuclear polarization is lost due to nuclear dipole-dipole interactions, so our model must suppress B_N around $B_{ext} = 0$, hence the first part of Property 2 [12]. The need for the second part of Property 2 manifests dramatically in the data shown in Fig. 4(a,c), where peak +1 for the down sweep cuts off prematurely around 6 mT. This is because, despite Larmor precession, there is a nonzero time-averaged electron spin polarization that produces a Knight field which oscillates in direction and magnitude at the photoelastic modulator frequency (50 kHz). This results in optical nuclear magnetic resonance (optical NMR) in the vicinity of 6 mT [10, 18]. When $B_{ext} + B_N$ reaches a resonance, the nuclear polarization is lowered or eliminated and the RSA peak shifts away from the current external field, hence the peak cutoff.

Property 3 has no obvious theoretical basis that we know of, but the reversal of peak warping and peak shifts upon reversal of sweep direction is unambiguous. To the degree this model is found to be valid, this property's eventual explanation will be of great interest.

Fig. 3(a,b) show the output of a simulation that exhibits the peak warping behavior seen in Fig. 1(d,e) using the model heuristics with $T_N = 3$ s. This demonstrates how the peak warping arises naturally from these heuristics. To understand this, consider what happens during an external field sweep. As B_{ext} approaches a RSA peak from either direction, electron spin polarization rises, followed by B_N . The change in net field shifts the peak away, but this movement is limited by the need to maintain enough spin polarization to sustain B_N . When the peak is finally passed, the resulting drop in spin polarization causes a corresponding decrease in B_N that moves the peak back towards its original position and further drops spin polarization, further decreasing B_N , and so forth. The result is a sharp drop in signal until the next peak.

While the peak warping phenomenon can be explained by the quickly-varying DNP simulated in Fig. 3(a,b), the rest of the results suggest a slowly-varying B_N produced by a T_N on the order of at least tens of seconds. Fig. 3(c,d) show the output of the same simulation, but with B_N and T_N magnified by a factor of 2 and 8, respectively. Note that peak warping can only occur when B_N changes quickly enough in the vicinity of a RSA peak to offset the external field sweep rate, about 0.23 mT/s. As a result, a larger T_N produces the slower-building DNP effects that are apparent in the data in Figs. 4-6 but minimal peak warping. As a demonstration, another simulation with this second set of parameters is directly compared with experimental results in Fig. 5(c,d).

Fig. 4(a) presents the results of a field sweep upwards from zero field to 160 mT and back. Fig. 4(b,c) superimpose these peaks to allow examination of how each successive peak differs from the last during the up sweep and down sweep, respectively. Fig. 4(d) charts the shifts in peak location, and Fig. 4(e) shows these shifts for a lower pump power. Note that RSA itself produces a noticeable warping of high-field peaks in field sweeps [16], as can be seen most clearly in the shape of the higher-numbered peaks. This warping effect was isolated and corrected for in Fig. 4(d,e). As noted earlier, the shift of each peak serves as a direct measurement of B_N , so Fig. 4(d,e) measures the trend of B_N across many peaks. Despite the variations in B_N around each peak that produce peak warping, on average B_N steadily rises over the course of the sweep, with a much stronger effect at higher pump power (consistent with Property 1).

Taking Fig. 4(b-e) together, it appears that this slower change in DNP tapers off only after at least ~ 7 peaks, demonstrated by a slowdown in the change of both peak shift and peak shapes at about peak +6 for both up-sweeps and downsweeps. This is broadly consistent with simulations that use a T_N of ~ 20 -30 s. Fig. 3(c,d) meet this condition and demonstrate how a slowly-varying DNP can require sweeping past several peaks to reach a steady state. However, we must be clear that we do not know how to marry the slow-timescale changes in the peak shape seen in Fig. 4(b,c) to the fast-timescale

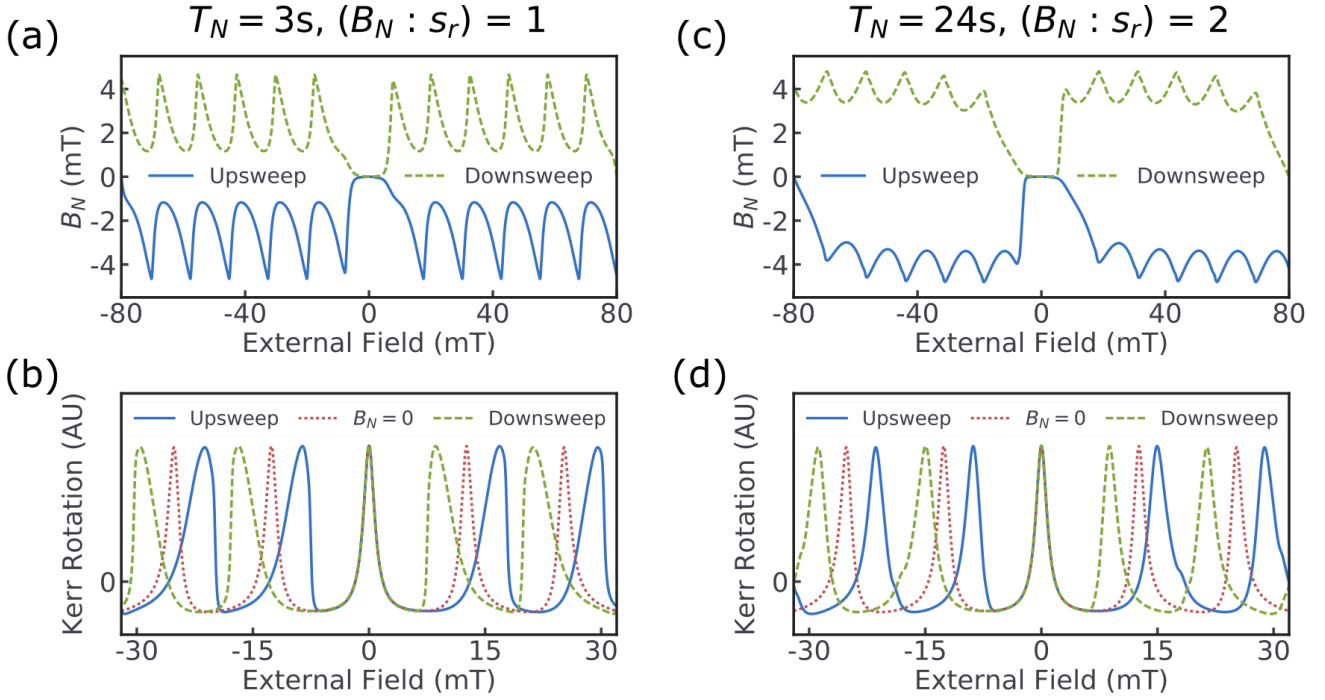


FIG. 3. (a) Overhauser field B_N (in mT) due to nuclear polarization as a function of external magnetic field and field sweep direction, modeled as described in the text. The field attempts to maintain a magnitude proportional to the total electron spin polarization, varying on the time scale of seconds. (b) Kerr Rotation as a function of external magnetic field swept up or down in the presence of dynamic nuclear polarization. The model reproduces the peak warping observed in Fig. 1(d). The case of $B_N = 0$ (no DNP) is shown by the dotted line. (c), (d) The model shown in (a) and (b) is reproduced with the magnitude of the Overhauser field doubled and the time scale on which DNP changes increased by a factor of 8. The peaks in (d) do not exhibit as significant a warping as observed in Fig. 1(d), though these simulation parameters better reflect the observed data in Fig. 5(a,b).

changes in B_N needed to produce those exaggerated peak shapes in the first place, as shown by the lack of peak warping in Fig. 3(d).

Comparing Fig. 4(b) with Fig. 4(c), we see that despite opposite trends in the warping of peak shape due to RSA, each successive peak measured (indicated by the direction of the arrow) grows shorter, wider, and further shifted from the no-DNP baseline than the last. This occurs regardless of whether the new peak corresponds to a higher or lower field than the last, as Fig. 4(d,e) demonstrate. From this evidence we conclude that the explanation for the peak shifts must depend on how much of the sweep has elapsed - the number of peaks passed, the time elapsed during the sweep, etc. - rather than directly depending on the strength of the external field. We suspect this condition rules out most other potential explanations for the data.

For example, Heisterkamp *et al.* explain their results in ZnSe using a periodic DNP model [10]. In that model, only the proximity of the current external field to a nuclear species NMR resonance field affects DNP strength. This is not a problem for explaining their own measurements because they do not report any difference in their results for sweeps of increasing versus decreasing field. However, for the reasons described in the previous para-

graph, this property would make a GaAs equivalent of their model inadequate to describe the data in Fig. 4.

It is important to note that the measurements of peak shift in Fig. 4(d,e) depend on the precise g-factor used to derive the reference peak locations, and different choices of wavelength produce subtle changes in apparent g-factor. As a further barrier to precise determination of the g-factor, even small pump powers resulted in a small but significant DNP at the wavelength used, obfuscating the g-factor derived from RSA peak spacing. The g-factor used in Fig. 2 and Fig. 4 was chosen to minimize the shift of peak 12 of the downsweep in Fig. 4(e), as a low power, high field, minimal DNP peak is ideal for measuring the g-factor from field sweep data. This condition also maximizes upsweep/downsweep peak change symmetry, though this exists to a large degree regardless of the g-factor choice.

The experiments shown in Figs. 5 and 6 demonstrate that any long-timescale B_N must rise and fall with the RSA peaks. In the experiment, the magnetic field sweep is paused for two minutes at various external field values. We measure the Kerr rotation while the external field is stationary (the steep period) before resuming the sweep. In Fig. 5(b) we steep on the rising edge of a RSA peak, and the Kerr rotation falls exponentially with a

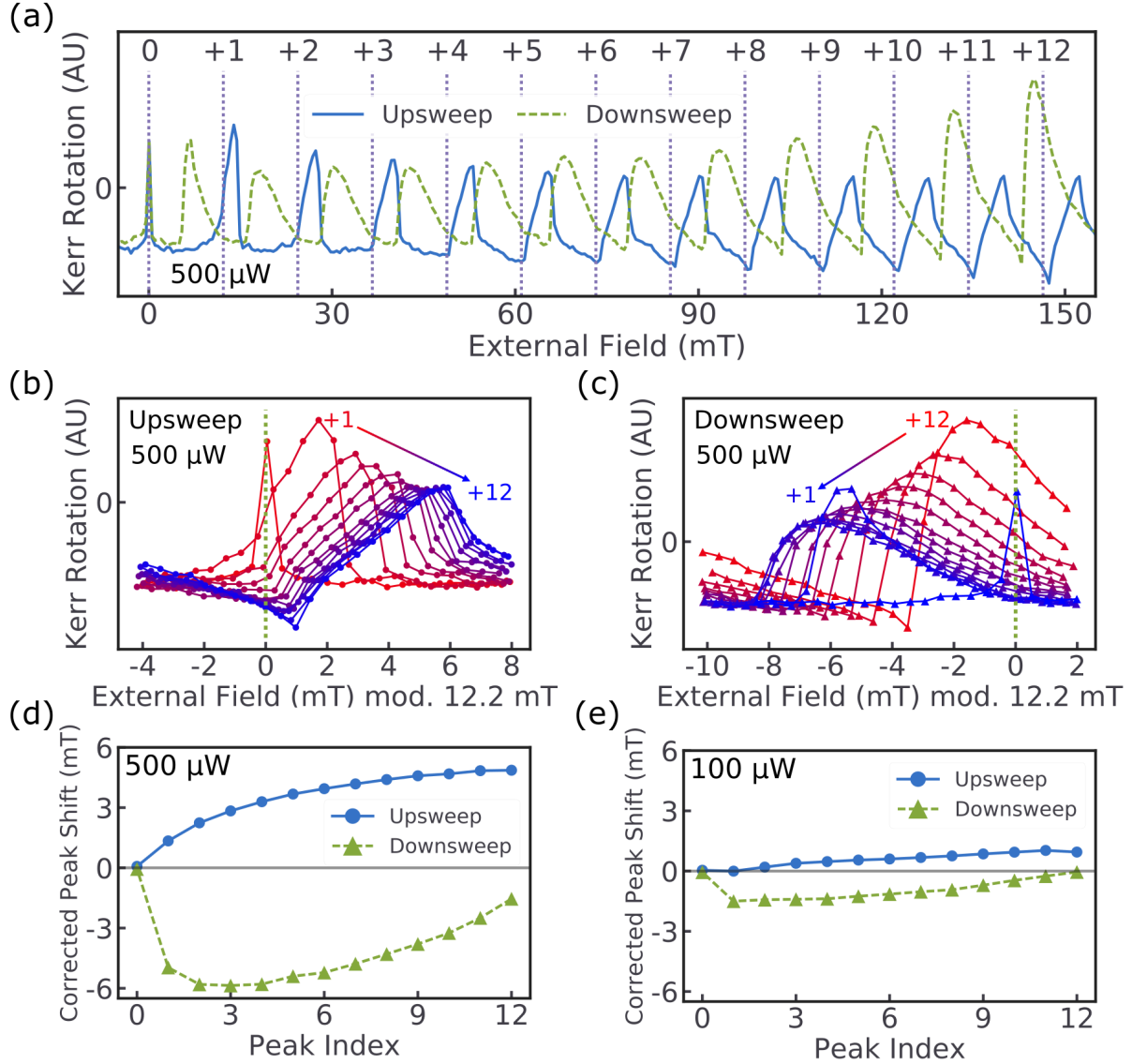


FIG. 4. (a) Kerr rotation measured as a function of external magnetic field for a fixed pump-probe delay of 13 ns. The field is swept from -160 mT to +160 mT for upsweeps and from +160 mT to -160 mT for downsweeps, but only the field range 0 mT to +160 mT is shown. The peaks are numbered with respect to the peak at zero applied field, as in Fig. 2(c,d). The dotted vertical lines indicate the expected positions of the RSA peaks in the absence of DNP. (b), (c) Peaks +1 through +12 plotted together as a function of external magnetic field modulo the expected peak spacing of 12.2 mT for field (b) upswipe and (c) downswipe. The dotted vertical line indicates the expected position of the RSA peaks in the absence of DNP. As both field sweeps progress, each successive RSA peak becomes more warped and shifts further away from the expected position. (d), (e) Corrected RSA peak shift as a function of peak index for incident pump power (d) 500 μW and (e) 100 μW . These shifts serve as a direct measurement of the Overhauser field B_N and demonstrate a symmetry between increasing and decreasing external magnetic field. The peak shift is more pronounced under higher incident pump power.

time constant on the order of 10-100 s. When the external field reaches the rising edge, the electron spin system has just emerged from its minimal polarization in the RSA trough, which was coupled with a corresponding drop in B_N . This increase in electron spin polarization now causes B_N to begin steadily rising during the steep. To see why this causes the observed drop in Kerr rotation, we will return to our earlier explanation of peak warping. During the steep the external field is static and

the peak slowly moves away, causing the observed drop in Kerr rotation. The Kerr rotation approaches an asymptotic limit as the peak moves far enough away that the electronic spin polarization is just strong enough to sustain its corresponding steady-state B_N . In contrast, Fig. 5(a) shows that when steeping while the external field is in a RSA trough, Kerr rotation actually rises slightly as B_N shrinks even more in the minimal electron spin polarization. Fig. 5(c,d) simulates the behaviors of Fig.

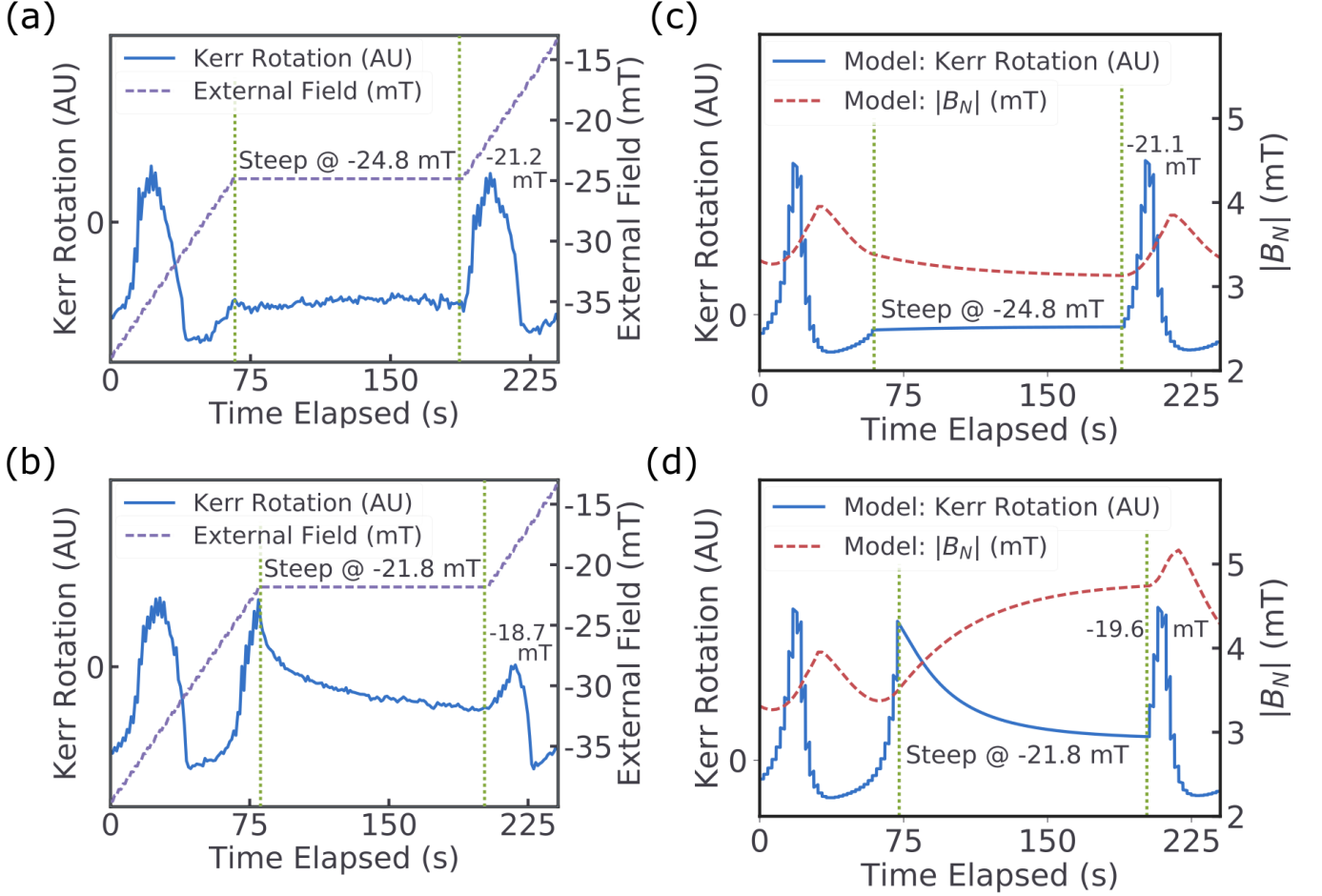


FIG. 5. (a), (b) Kerr rotation (solid line) measured as a function of time elapsed during a field sweep, for a fixed pump-probe delay of 13 ns. The external magnetic field (dashed line) is swept up from -80 mT, incremented at a rate of about 0.23 mT/s, to the desired steep field and held constant for two minutes. The field is then swept up to +25 mT, though only a portion of each field sweep is shown here for clarity. Data is shown for steep fields (a) in the trough between RSA peaks and (b) on the rising edge of a RSA peak. In (a), Kerr rotation increases slightly as the external field is held constant; in (b), Kerr rotation decays exponentially with a time scale on the order of 10-100 s. The peak location changes as a result of steeping, as shown by the labeled peaks. (c), (d) Simulated Kerr rotation (solid line) as a function of time elapsed corresponding to the steep sweeps outlined in (a) and (b), respectively. The dashed line shows the modeled nuclear field. The model reproduces the decay in Kerr rotation in (b) as well as the changes in peak location as a result of steeping (peaks labeled).

5(a,b) using the same model parameters that were used in Fig. 3(c,d). The peak after the steep is also displaced in proportion to the rise of B_N during the steep, confirming the peak shifting away explanation for the drop in Kerr rotation.

Fig. 6 provides more evidence that B_N indeed rises and falls with the electron spin polarization as described in the last paragraph. Fig. 6(f) shows that without any steeping, a peak occurs at $B_{ext} = -21.2$ mT. However, Fig. 6(a-d) show that steeping successively closer to that peak results in the peak being pushed back increasingly further, to a maximum extra peak shift of +2.5 mT when the steep occurs at -21.8 mT, right at the cusp of the peak and where electron spin polarization is maximized. This extra peak shift is a direct measurement of how much B_N rose during the steep, and we can see that

this can vary between zero and 2.5 mT based on the electron spin polarization at which the steep occurred. Furthermore, this can be done with the same results on any peak for increasing or decreasing B_{ext} , so clearly the trajectory of B_N varies in a complex way based on the precise external field history of the system down to the mT level, providing compelling evidence for Property 1.

The other notable feature of Fig. 6 is the strange behavior of the peak at $B_{ext} \approx -10$ mT. The precise location of the steep on the previous RSA peak causes a striking change in the shape of this peak, even splitting the peak in two. In this case only one peak remained before B_N was erased in the vicinity of $B_{ext} = 0$, but in the general case this peak deformation occurs on all peaks subsequent to the steep, albeit to a lesser degree with each successive peak. We do not attempt to explain this steep

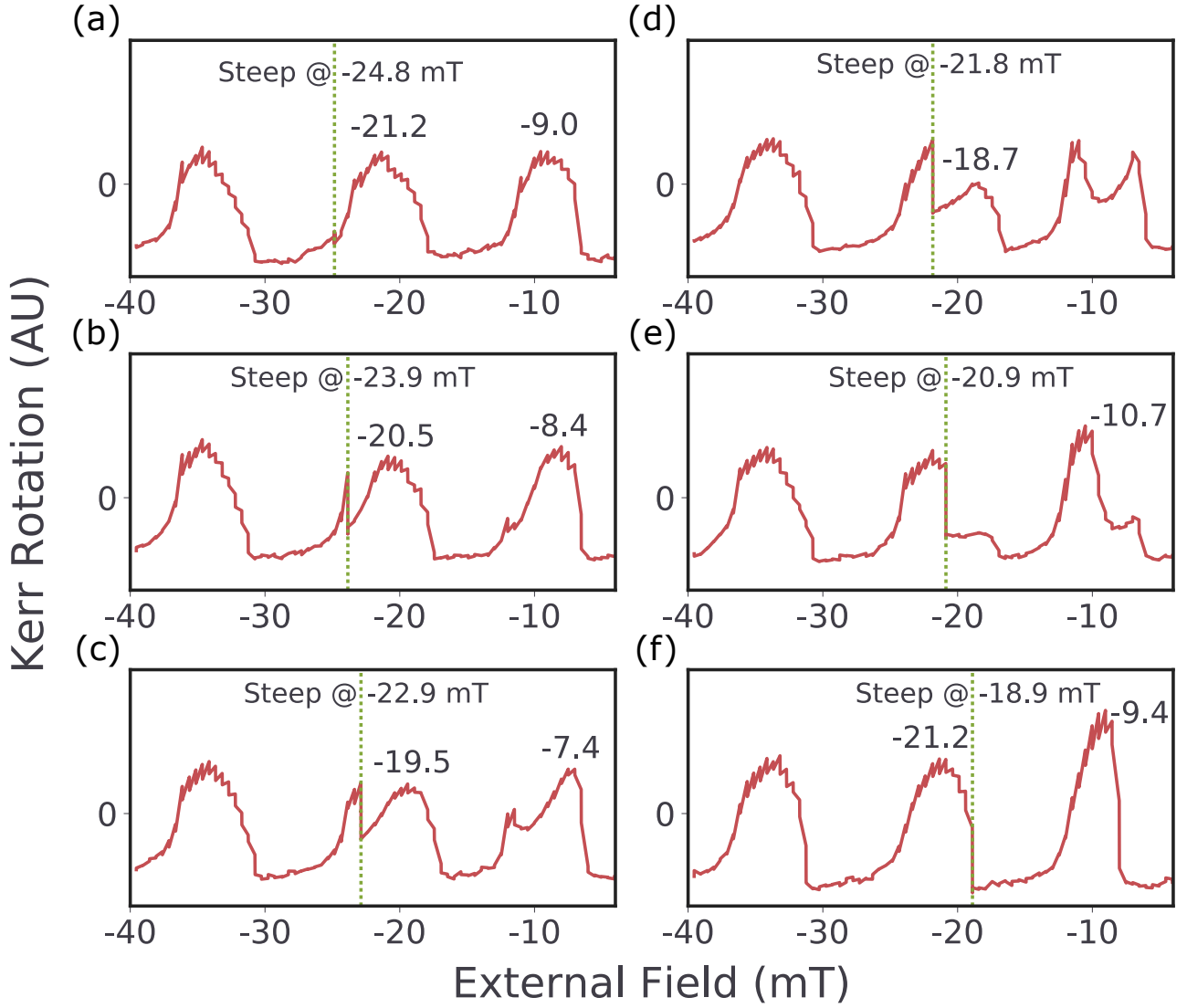


FIG. 6. (a)-(f) Kerr rotation measured as a function of external magnetic field, for a fixed pump-probe delay of 13 ns. The external magnetic field is swept up from -80 mT, incremented at a rate of about 0.23 mT/s, to the desired steep field and held constant for two minutes. The field is then swept up to +25 mT, though only peaks -3, -2, and -1 are shown. The chosen steep field influences the locations of peak -2, as shown by the labels, with steep fields close to the maximum of peak -2 yielding the greatest shift. Steep field (a) -24.8 mT is far enough from the center of peak -2 to not cause that peak to shift, as is evident by comparison to (f) -18.9 mT. Furthermore, peak -1 is heavily deformed in accordance with the chosen steep field, so as to echo the shape of peak -2.

echo behavior here, but we are currently examining the effect further.

IV. CONCLUSION

We have shown the existence of DNP that varies in magnitude with the net electron spin polarization generated by the resonant amplification or nullification of successive packets of optically-generated electron spins. Furthermore, this nuclear polarization is parallel to the external magnetic field and perpendicular to the electron spins upon which it depends. The phenomenologi-

cal model we present captures the subtle time-dependent behaviors of the nuclear polarization. To the degree this model is accurate it raises the mystery of the apparent difference in nuclear polarization for increasing versus decreasing fields. Finally, we show that steeping during a sweep of external magnetic field produces a mysterious echo effect in the subsequent spin signal that warrants further investigation.

ACKNOWLEDGMENTS

The authors would like to thank Hua-Wei Hsu and Mayank Goyal for their contributions. J.R.I. was supported by the Department of Defense through the National Defense Science and Engineering Graduate Fellow-

ship (NDSEG) program. The work at the University of Michigan is supported by the National Science Foundation under Grant No. DMR-1607779. Sample fabrication was performed at the University of Michigan Lurie Nanofabrication Facility.

-
- [1] J. A. Reimer, *Nuclear hyperpolarization in solids and the prospects for nuclear spintronics*, Solid State Nuclear Magnetic Resonance **37**, 3-12 (2010).
 - [2] B. Urbaszek, X. Marie, T. Amand, O. Krebs, P. Voisin, P. Maletinsky, A. Högele, and A. Imamoglu, *Nuclear spin physics in quantum dots: An optical investigation*, Rev. Mod. Phys. **85**, 79-133 (2013).
 - [3] R. J. Warburton, *Single spins in self-assembled quantum dots*, Nature Materials **12**, 483-493 (2005).
 - [4] E. A. Chekhovich, M. N. Makhonin, A. I. Tartakovskii, A. Yacoby, H. Bluhm, K. C. Nowack, and L. M. K. Vandersypen, *Nuclear spin effects in semiconductor quantum dots*, Nature Materials **12**, 494-504 (2013).
 - [5] G. Lampel, *Nuclear dynamic polarization by optical electronic saturation and optical pumping in semiconductors*, Phys. Rev. Lett. **20**, 491-493 (1968).
 - [6] J. M. Kikkawa and D. D. Awschalom, *All-optical magnetic resonance in semiconductors*, Science **287**, 473-476 (2000).
 - [7] G. Salis, D. T. Fuchs, J. M. Kikkawa, D. D. Awschalom, Y. Ohno, and H. Ohno, *Optical manipulation of nuclear spin by a two-dimensional electron gas*, Phys. Rev. Lett. **86**, 2677 (2001).
 - [8] D. Gammon, Al. L. Efros, T. A. Kennedy, M. Rosen, D. S. Katzer, D. Park, S. W. Brown, V. L. Korenev, and I. A. Merkulov, *Electron and nuclear spin interactions in the optical spectra of single GaAs quantum dots*, Phys. Rev. Lett. **86**, 5176 (2001).
 - [9] E. A. Zhukov *et al.*, *All-optical NMR in semiconductors provided by resonant cooling of nuclear spins interacting with electrons in the resonant spin amplification regime*, Phys. Rev. B **90**, 085311 (2014).
 - [10] F. Heisterkamp, A. Greilich, E. A. Zhukov, E. Kirstein, T. Kazimierzczuk, V. L. Korenev, I. A. Yugova, D. R. Yakovlev, A. Pawlis, and M. Bayer, *Inhomogeneous nuclear spin polarization induced by helicity-modulated optical excitation of fluorine-bound electron spins in ZnSe*, Phys. Rev. B **92**, 245441 (2015).
 - [11] E. A. Zhukov, E. Kirstein, N. E. Kopteva, F. Heisterkamp, I. A. Yugova, V. L. Korenev, D. R. Yakovlev, A. Pawlis, M. Bayer and A. Greilich, *Discretization of the total magnetic field by the nuclear spin bath in fluorine-doped ZnSe*, Nature Commun. **9**, 1941 (2018).
 - [12] F. Meier and B. P. Zakharchenya (eds.), *Optical Orientation* (Elsevier, Amsterdam, 1984).
 - [13] X. Xu, W. Yao, B. Sun, D. G. Steel, A. S. Bracker, D. Gammon, and L. J. Sham, *Optically controlled locking of the nuclear field via coherent dark-state spectroscopy*, Nature **459**, 1105-1109 (2009).
 - [14] I. Vink, K. Nowack, F. Koppens, J. Danon, Y. Nazarov, and L. Vandersypen, *Locking electron spins into magnetic resonance by electron-nuclear feedback*, Nature Physics **5**, 764-768 (2009).
 - [15] S. A. Crooker, D. D. Awschalom, J. J. Baumberg, F. Flack, and N. Samarth, *Optical spin resonance and transverse spin relaxation in magnetic semiconductor quantum wells*, Phys. Rev. B **56**, 7574 (1997).
 - [16] J. M. Kikkawa and D. D. Awschalom, *Resonant spin amplification in n-type GaAs*, Phys. Rev. Lett. **80**, 4313-4316 (1998).
 - [17] C. J. Trowbridge and V. Sih, *Phase effects due to previous pulses in time-resolved Faraday rotation measurements*, J. Appl. Phys. **117**, 063906 (2015).
 - [18] R. K. Kawakami, Y. Kato, M. Hanson, I. Malajovich, J. M. Stephens, E. Johnston-Halperin, G. Salis, A. C. Gosard, and D. D. Awschalom, *Ferromagnetic imprinting of nuclear spins in semiconductors*, Science **294**, 131-134 (2001).